Available online at www.sciencedirect.com
SCIENCE DIRECT®
Journal of Catalysis 220 (2003) 347–357
JOURNAL OF CATALYSIS
www.elsevier.com/locate/jcat

Characterizations and catalytic properties of Cr-MCM-41 prepared by direct hydrothermal synthesis and template-ion exchange

Ye Wang,[a,*] Yoshihiko Ohishi,[b] Tetsuya Shishido,[c] Qinghong Zhang,[a] Wei Yang,[a] Qian Guo,[a] Huilin Wan,[a] and Katsuomi Takehira [b]

[a] *State Key Laboratory for Physical Chemistry of Solid Surfaces, Department of Chemistry, Xiamen University, Xiamen 361005, China*
[b] *Department of Chemistry and Chemical Engineering, Graduate School of Engineering, Hiroshima University, Higashi-Hiroshima 739-8527, Japan*
[c] *Department of Chemistry, Tokyo Gakugei University, Koganei, Tokyo 184-8501, Japan*

Received 17 March 2003; revised 9 June 2003; accepted 16 June 2003

Abstract

Cr-MCM-41 prepared by direct hydrothermal synthesis (DHT) and template-ion exchange (TIE) has been characterized by X-ray diffraction (XRD), N_2 adsorption (77 K), diffuse reflectance UV–vis, X-ray absorption (XANES and EXAFS), and UV-Raman spectroscopic measurements. It is suggested that monochromate species mainly exist on the Cr-MCM-41 by the DHT method while several types of chromate species including both monochromates and polychromates coexist on that by the TIE method. The two kinds of samples exhibit similar catalytic property in the dehydrogenation of propane with carbon dioxide. The selectivity to propylene is higher than 90% and the presence of carbon dioxide enhances propane conversion. The chromate species on both types of samples are reduced to aggregated Cr(III) with octahedral coordination during the dehydrogenation reactions. On the other hand, the selectivity to formaldehyde in the partial oxidation of methane with oxygen is remarkably higher over the sample by the DHT method than that by the TIE method. The structure of the chromate species is kept during the oxidation of methane, and the high dispersion of monochromate species probably accounts for the higher selectivity over the sample by the DHT method.

Keywords: Cr-MCM-41; Chromate species; Dehydrogenation; Propane; Methane; Partial oxidation

1. Introduction

Chromium-based catalysts have received much attention because of their wide use in many catalytic reactions [1,2]. Silica- and alumina-supported chromium oxides were industrially used for the production of polyethylene (Phillips catalyst) [3,4] and lower alkenes such as propylene and isobutene through the dehydrogenation of the corresponding alkanes [5,6], respectively. Carbon dioxide was found to enhance the dehydrogenation of propane [7] or ethane [8,9] over silica-supported chromium oxide. Supported chromium oxides have also been investigated for the oxidative dehydrogenation of lower alkanes [10–13] or oxidation of other organic compounds with oxygen [14,15]. The redox property and the appropriate dispersion of chromium species on the support are important in these catalytic reactions [13].

Studies of chromium species introduced into MCM-41, a typical mesoporous molecular sieve, would thus be useful in developing Cr-containing catalysts with desirable catalytic properties. There exist several studies on the syntheses and characterizations of Cr-MCM-41 [16–21]. For catalytic reactions, Cr-MCM-41 has been used for the liquid-phase oxidation with alkyl hydroperoxide [21] or hydrogen peroxide [22], but the leaching of chromium to the liquid phase seems a big problem for the Cr-containing microporous and mesoporous materials [23–25]. Cr-containing mesoporous molecular sieves (Cr-HMS) were reported to exhibit high photocatalytic reactivity in ethylene polymerization [26]. Cr-MCM-41 prepared by an impregnation method was once used for the oxidative dehydrogenation of propane with oxygen, but the selectivity to propylene was low (18.4% at 12.4% propane conversion) and the yield to propylene was lower than 5% [20]. Recently, a SBA-15-supported chromium oxide by the impregnation method has been applied to the dehydrogenation and the oxidative

* Corresponding author.
E-mail address: yewang@jingxian.xmu.edu.cn (Y. Wang).

0021-9517/$ – see front matter
doi:10.1016/S0021-9517(03)00278-1

dehydrogenation of propane and showed good catalytic performance [27].

The oxidation state of chromium and the coordination structure of chromium species over supported chromium oxides and Cr-containing molecular sieves have been investigated by various techniques such as ESR [28], UV–vis diffuse reflectance spectroscopy [29], XPS [30], XANES [21,31], and TPR [32]. Several types of chromium species, e.g., monochromate, polychromate, and aggregated chromium oxide have been reported to exist on these samples.

It can be expected that different synthetic methods would result in different chromium species and the different chromium species may behave differently in catalytic reactions. Although there are many studies on the correlation between catalytic properties and coordination structures of the supported chromium oxides [33], such structure-property relationships are still needed to elucidate the Cr-containing mesoporous molecular sieve systems in different types of reactions. Recently, we applied two different methods, i.e., direct hydrothermal synthesis (DHT) and template-ion exchange (TIE), to the syntheses of V- [34], Fe- [35], and Mn-MCM-41 [36]. The two methods resulted in different locations and coordination environments of the incorporated metal cations; the TIE method provided highly dispersed metal ions on the wall surface of MCM-41 inside the mesopores and the DHT method had the tendency to incorporate metal ions inside the framework of MCM-41. It has been clarified that the two different methods for introducing metal ions bring about remarkably different catalytic behaviors in selective oxidation reactions.

In the present paper, we report the synthesis of Cr-MCM-41 using the TIE and the DHT methods. The synthesized materials are characterized in detail to gain information about the structures of the introduced chromium species. Two kinds of catalytic reactions, viz., the dehydrogenation of propane with carbon dioxide and the partial oxidation of methane with oxygen are investigated and compared to elucidate the structure-property relationships for the two types of Cr-MCM-41.

2. Experimental

2.1. Materials

Chromium was introduced into MCM-41 by following two different methods. The Cr-MCM-41-DHT was prepared by direct hydrothermal synthesis. Chromium nitrate, sodium silicate, and hexadecyltrimethylammonium bromide were used as the sources of chromium, silicon, and the template, respectively. The molar ratio of the template to the silicon source was kept at 0.5 in the synthesis gel for each synthesis. The synthesis gel was stirred for 1 h at room temperature and was then transferred to a Teflon bottle, which was placed in a stainless-steel autoclave after the adjustment of the pH value of the mixed gel to 10.5 with 4 M HCl. The hydrothermal synthesis was carried out at 150 °C for 48 h, and then the resultant solid was recovered by filtration, washed with deionized water thoroughly, and dried at 40 °C in vacuum for ca. 24 h. After calcination at 550 °C for 6 h in a flow of dry air, the Cr-MCM-41-DHT was obtained. The Cr-MCM-41-TIE was synthesized by the template ion-exchange method. It is known that the cationic surfactants in the as-synthesized MCM-41 after hydrothermal synthesis are mainly organized in the form of a cylindrical micellar structure with hydrophilic positive ends interacting with silica pore surfaces via Coulombic interaction, and can be replaced through the ion-exchange by other cations such as VO^{2+} [34,37], Fe^{3+} [35,38], Mn^{2+} [36, 39,40], Ti [40], $[Co(en)_2Cl_2]^+$ [41], and other positively charged complexes. In our experiments, typically the as-synthesized MCM-41 (2 g) containing ca. 50 wt% template was added to an ethanolic solution of chromium nitrate and stirred vigorously at 60 °C for 6 h for ion exchanging between the cationic template and the Cr^{3+} ion. After the ion exchange, the as-synthesized Cr-MCM-41-TIE was recovered by filtration, washing thoroughly with deionized water, and drying at 40 °C in vacuum. The remained organic template was removed by calcination at 550 °C for 6 h to gain the Cr-MCM-41-TIE sample.

2.2. Characterizations

Inductively coupled plasma (ICP) optical emission spectrometry was used for the determination of the chromium content in each sample synthesized above. The measurements were performed with a Perkin-Elmer OPTIMA 3000, and the sample was dissolved in a mixture of HF and HNO_3 acids before the measurement.

N_2-adsorption studies were used to examine the porous properties of each sample. The measurements were carried out on Belsorp 18SP equipment (volumetric), and all the samples were pretreated in vacuum at 200 °C for 12 h before the measurement. The pore-size distribution was evaluated from the adsorption isotherm by the Dollimore and Heal (DH) method [42].

X-ray diffraction (XRD) patterns were collected on a SRA M18XHF diffractometer (MAC Science Co., Ltd., Japan) with Cu-K_α radiation (40 kV, 300 mA). Small divergent and scattering slits (0.05 mm) were selected to avoid a high background at low diffraction angles.

Diffuse reflectance UV–vis spectra were recorded on a Perkin-Elmer Lambda 900 UV/VIS/NIR spectrometer. The powdery sample was loaded into a quartz cell, and the spectra were collected at 200–700 nm referenced to $BaSO_4$.

X-ray absorption spectroscopic measurements were performed with synchrotron radiation at a beam line BL7C station of the photon factory, at the High Energy Accelerator Research Organization (Tsukuba, Japan), operated at 2.5 GeV with about 350–380 mA of ring current. The data were recorded in X-ray fluorescence mode at room temperature using a Si(111) double crystal monochromator. Energy

was calibrated with CuK-edge absorption (8981.0 eV), and the energy step of measurement in the XANES region was 0.3 eV. The absorption was normalized to 1.0 at an energy position of 30 eV higher than the absorption edge.

UV-Raman spectroscopic measurements were carried out with a Renishaw UV–vis Raman System 1000R using the UV line at 325 nm from a Kimmon IK 3201R-F He-Cd laser as the exciting source. The sample was loaded in an in situ cell and was treated in pure N_2 gas flow at 200 °C for dehydration before the measurement. A laser output of 30 mW was used and the maximum incident power at the sample was approximately 6 mW.

2.3. Catalytic properties

The dehydrogenation of C_3H_8 with CO_2 and the partial oxidation of CH_4 with O_2 were investigated, respectively, to study the catalytic properties of the materials synthesized above. Both kinds of reactions were carried out using a fixed-bed flow reactor (U-type quartz tube with inner diameter of 4 mm) operated at atmospheric pressure.

In the dehydrogenation reactions, typically 0.4 g of sample, which had been pelletized and sieved to 250–417 μm, was loaded into the reactor and treated in a gas flow containing N_2 (10 ml min^{-1}) and O_2 (10 ml min^{-1}) at 550 °C for 1 h and then purged with He (purity, 99.99%). The reaction was started by introducing a gas mixture of CO_2, C_3H_8, He, and N_2 to the reactor. N_2 was used as the internal standard for the calculations of the conversions of CO_2 and C_3H_8, while He was used for dilution to control the partial pressures of the reactants.

For partial oxidation of CH_4, typically 0.05 g of sample was used. After pretreatment at 550 °C in a flow of mixture of He (50 ml min^{-1}) and O_2 (10 ml min^{-1}) for 1 h, the reactants of CH_4 and O_2 diluted with He were fed to the reactor to start the reaction. The products in each reaction were analyzed by on-line gas chromatography. All the lines and valves between the exit of the reactor and the gas chromatographs were heated to 120 °C to prevent the condensation of the partial oxidation products.

3. Results and discussion

3.1. Porous properties of materials

Fig. 1 shows the XRD patterns at low diffraction angles for the calcined Cr-MCM-41 samples with Si/Cr atomic ratios of 100 and 50 prepared by both the DHT and the TIE methods. Four diffraction lines at 2θ degrees of 2–6° indexed to (100), (110), (200), and (210) of the regularity of hexagonal array of mesopores of MCM-41 were observed for all these samples. The peak intensities for the Cr-containing MCM-41 samples were not significantly lowered as compared with those for the purely silicious MCM-41, suggesting that the long-range regularity of hexagonal

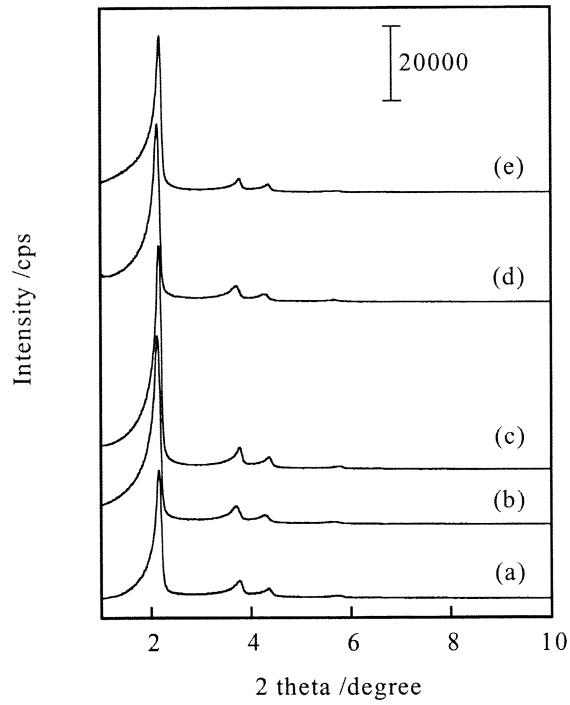

Fig. 1. XRD patterns at low diffraction angles for the Cr-MCM-41 samples prepared by both DHT and TIE methods. (a) MCM-41; (b) DHT, Si/Cr = 100; (c) TIE, Si/Cr = 100; (d) DHT, Si/Cr =50; (e) TIE, Si/Cr = 50.

arrays of mesopores of MCM-41 was sustained after the introduction of chromium up to a content of 1.7 wt% (Si/Cr = 50) by both methods. However, as Si/Cr ratio decreased to 25, in other words, as the chromium content increased to 3.4 wt%, these diffraction peaks decreased largely for the samples prepared by both methods, indicating a decrease in the structural regularity of the mesoporous structure at higher chromium content. XRD results at high diffraction angles for the calcined Cr-MCM-41 samples with a Si/Cr ratio of 25 are shown in Fig. 2. Only a broad peak due to amorphous feature of the framework of MCM-41 appeared. Any peak assignable to the crystalline Cr_2O_3 phase was not observed for the Cr-MCM-41 samples prepared by both methods.

The porous properties obtained from N_2 adsorption at 77 K are shown in Table 1. For both series of materials, the surface area and pore volume gradually decreased with an increase in chromium content up to 1.7 wt% (Si/Cr = 50), and became remarkably low as the chromium content was increased to 3.4 wt% (Si/Cr = 25). The drop in the surface area and the pore volume at such high chromium content was consistent with the decrease in structural regularity observed by XRD. No significant difference between the TIE and the DHT samples was observed.

3.2. Coordination structure of chromium

3.2.1. XANES results

Fig. 3A shows the CrK-edge XANES spectra of several reference compounds. Chromium atoms in Na_2CrO_4,

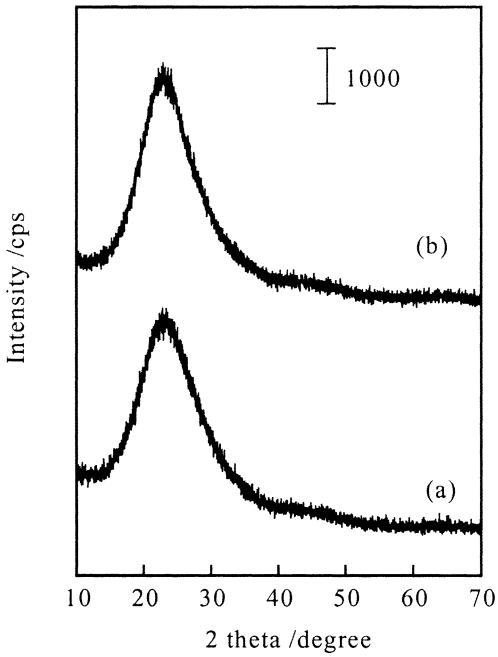

Fig. 2. XRD patterns at high diffraction angles for the Cr-MCM-41 samples with a Si/Cr ratio of 25. (a) DHT method; (b) TIE method.

Table 1
Porous properties of Cr-MCM-41 samples synthesized by the DHT and the TIE methods

Sample[a]	BET surface area ($m^2\,g^{-1}$)	Pore volume ($cm^3\,g^{-1}$)	Pore diameter (nm)
MCM-41	1025	0.89	2.7
Cr-MCM-41-DHT(100)	878	0.79	2.7
Cr-MCM-41-DHT(50)	780	0.70	2.7
Cr-MCM-41-DHT(25)	629	0.36	2.7
Cr-MCM-41-TIE(100)	961	0.92	2.7
Cr-MCM-41-TIE(50)	885	0.83	2.7
Cr-MCM-41-TIE(25)	624	0.55	2.5

[a] The numbers in parentheses are the Si/Cr atomic ratios.

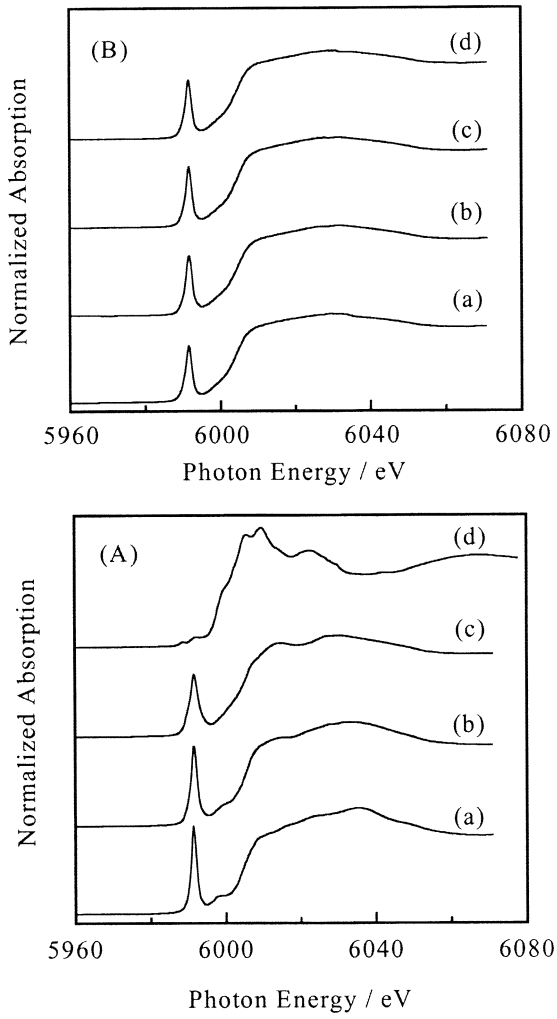

Fig. 3. Cr*K*-edge XANES spectra of the reference compounds (A) and the Cr-MCM-41 samples (B). (A): (a) Na_2CrO_4; (b) $K_2Cr_2O_7$; (c) CrO_3; (d) Cr_2O_3. (B): (a) DHT, Si/Cr = 100; (b) DHT, Si/Cr = 50; (c) TIE, Si/Cr = 100; (d) TIE, Si/Cr = 50.

$K_2Cr_2O_7$, and CrO_3 are all in tetrahedral coordination whereas those in Cr_2O_3 are octahedrally coordinated with oxygen. The preedge peak at ca. 5991 eV is attributed to the so-called 1s–3d dipole forbidden transition, and this forbidden transition principally gains additional intensity when the chromium center is in a noncentral symmetric environment or through mixing of 3d and 4p orbitals caused by the breakdown of inversion symmetry due to structure distortion. Since the local symmetry around the metal center is lowered from octahedral to tetrahedral coordination, the intensity of the preedge peak tends to increase simultaneously, i.e., $I_{\text{octahedral}} < I_{\text{square pyramidal}} < I_{\text{tetrahedral}}$ [43]. Fig. 3A clearly shows that the compounds with tetrahedrally coordinated chromium exhibit remarkably higher intensity of the preedge peak. Fig. 3A also reveals that the edge position shifts with the change in oxidation state; the edge position for Cr_2O_3 with Cr(III) is at 5997.6 eV, while those for CrO_3, $K_2Cr_2O_7$, and Na_2CrO_4 with Cr(VI) shift to 6006.0, 6006.3, and 6004.6 eV. The XANES results for these reference compounds shown here are very similar to those reported by Haller and co-workers [31].

Fig. 3B shows the Cr*K*-edge XANES spectra of the Cr-MCM-41 samples by both the DHT and the TIE methods. No significant difference between the samples by the DHT and the TIE methods could be seen from the XANES results. The comparison of these spectra with those for the references suggests that the chromium on each Cr-MCM-41 sample exists as the chromate species with Cr(VI) in tetrahedral coordination.

3.2.2. EXAFS results

Fig. 4 shows the Fourier transforms of k^3-weighted Cr*K*-edge EXAFS spectra of the reference compounds. Three main peaks at 1.62, 2.58, and 3.29 Å (non-phase-shift corrected) were observed for Cr_2O_3, and these three peaks corresponded to the bonds of Cr–O in CrO_6 octahedra, Cr–O–Cr through edge-shared CrO_6 octahedra, and Cr–O–Cr through corner-shared CrO_6 octahedra, respectively [44].

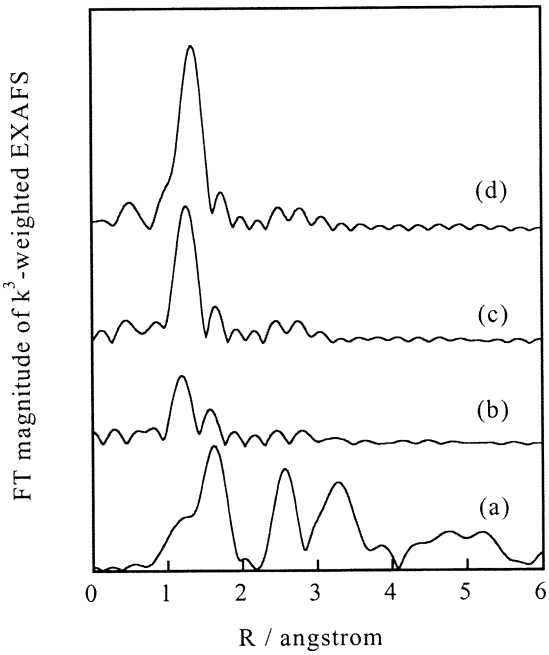

Fig. 4. Fourier transforms of k^3-weighted CrK-edge EXAFS of reference compounds. (a) Cr_2O_3, (b) CrO_3, (c) $K_2Cr_2O_7$, (d) Na_2CrO_4.

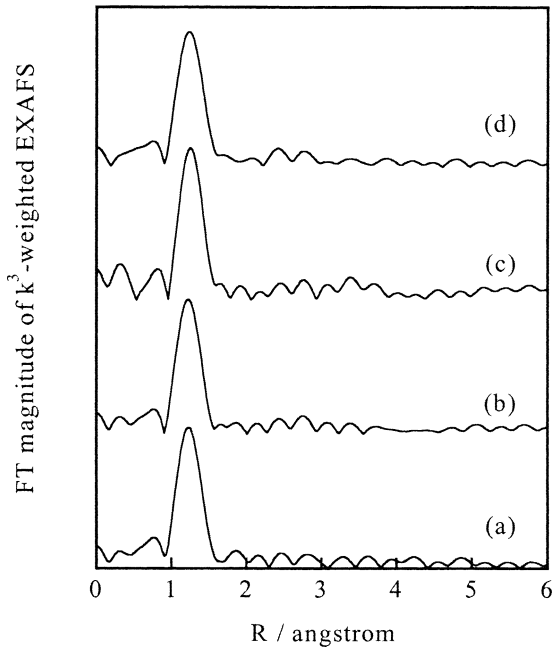

Fig. 5. Fourier transforms of k^3-weighted CrK-edge EXAFS of the Cr-MCM-41 samples. (a) DHT, Si/Cr = 100; (b) DHT, Si/Cr = 50; (c) TIE, Si/Cr = 100; (d) TIE, Si/Cr = 50.

For CrO_3, $K_2Cr_2O_7$, and $NaCrO_4$ with Cr(VI) in CrO_4 tetrahedra, the main peak for the Cr–O bond was observed at 1.20–1.35 Å (non-phase-shift corrected), coinciding with the shortened bond distance of Cr–O in CrO_4 tetrahedron. The intensity of the EXAFS oscillation for CrO_3 was quite weaker than those for Na_2CrO_4, $K_2Cr_2O_7$, and Cr_2O_3 (not shown), suggesting the disorder of the CrO_4 tetrahedron in CrO_3. The significantly low intensity of the peak of Cr–O bond for CrO_3 as shown in Fig. 4 (curve b) was probably due to such disorder. The Cr–O–Cr bond could not be clearly seen in the spectra of these three compounds with tetrahedrally coordinated chromium although the Cr–O–Cr linkage is actually contained in $K_2Cr_2O_7$ and CrO_3. We attempted to analyze the second-shell neighbors, but the analysis of the Cr–O–Cr shells was not successful. In other words, our EXAFS measurements are not sensitive enough to clarify whether the Cr–O–Cr linkages exist in the chromate species.

The Fourier transforms of k^3-weighted CrK-edge EXAFS spectra of the Cr-MCM-41 samples by both the DHT and the TIE methods are shown in Fig. 5. Similar to the XANES results, no significant difference could be seen between the two types of samples by different methods. The peak of the Cr–O bond was observed at 1.23 Å (non-phase-shift corrected), suggesting that chromium atoms were in tetrahedral coordination.

The EXAFS parameters of the Cr–O shell are summarized in Table 2. Table 2 confirms the tetrahedral coordination of chromium (total coordination number = 3.9) for both types of samples after calcination. However, the four Cr–O bonds of the CrO_4 tetrahedron are not equivalent; two of the Cr–O bonds are shorter (1.66–1.67 Å) and the other two are relatively longer (1.85–1.87 and 2.01–2.01 Å, respectively). The two shorter Cr–O bonds may possess a double-bond nature and the other two possess a single-bond nature.

Table 2
Parameters obtained from EXAFS analysis for the calcined Cr-MCM-41 samples by the DHT and the TIE methods[a]

Sample[b]	Shell	C.N.	R (Å)	$\Delta\sigma^2$ (Å^2)
Cr-MCM-41-DHT(100)	Cr–O	2.0	1.66	−0.0052
	Cr–O	0.9	1.86	−0.0069
	Cr–O	1.0	2.02	0.0033
Cr-MCM-41-DHT(50)	Cr–O	2.0	1.66	−0.0047
	Cr–O	0.9	1.85	−0.0057
	Cr–O	1.0	2.01	0.0064
Cr-MCM-41-DHT(50)[c]	Cr–O	2.0	1.66	−0.0039
	Cr–O	0.9	1.86	−0.0046
	Cr–O	1.0	2.02	0.0053
Cr-MCM-41-DHT(50)[d]	Cr–O	3.0	1.97	−0.0005
	Cr–O	3.1	2.06	0.0016
Cr-MCM-41-TIE(100)	Cr–O	2.0	1.67	−0.0050
	Cr–O	0.9	1.87	−0.0054
	Cr–O	1.0	2.01	0.0114
Cr-MCM-41-TIE(50)	Cr–O	2.0	1.66	−0.0048
	Cr–O	0.9	1.86	−0.0045
	Cr–O	1.0	2.01	0.0085

[a] C.N., coordination number; R, bond length (Å); $\Delta\sigma^2$, Debye–Waller factor (Å^2).
[b] The numbers in parentheses are the Si/Cr atomic ratios.
[c] After pretreatment in He flow at 823 K for 1 h.
[d] After 5 h of reaction under the conditions shown in Fig. 8.

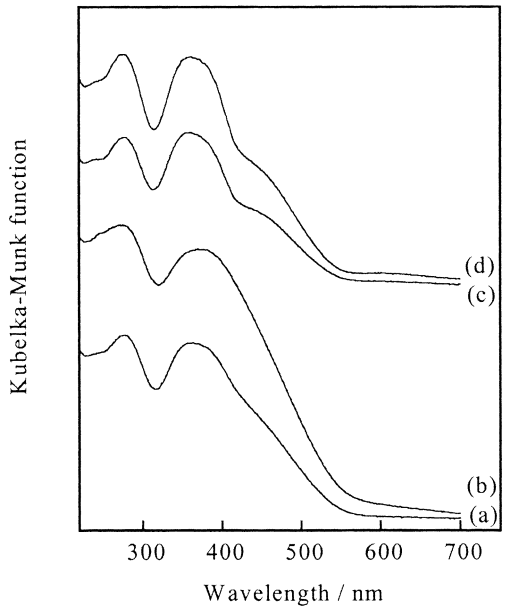

Fig. 6. Diffuse reflectance UV–vis spectra of the Cr-MCM-41 samples. (a) DHT, Si/Cr = 50; (b) DHT, Si/Cr = 25; (c) TIE, Si/Cr = 100; (d) TIE, Si/Cr = 50.

3.2.3. Diffuse reflectance UV–vis results

Fig. 6 shows the diffuse reflectance UV–vis spectra of the calcined Cr-MCM-41 synthesized by both methods. UV bands at 280 and 370 nm were mainly observed for both kinds of samples. These bands could be assigned to the O–Cr(VI) charge transfer of the chromate species [2]. The difference between the DHT and the TIE samples was not distinct, although it seems that a weak shoulder around 440 nm, characteristic of Cr(VI) polychromate, appeared for the TIE samples. The appearance of such a weak shoulder may indicate the existence of polychromate in the samples synthesized by the TIE method, but the large band at 370 nm may overlap the shoulder at 440 nm in the case of DHT samples.

3.2.4. UV-Raman results

Kevan and co-workers [19] once reported the Raman spectrum of a Cr-MCM-41 with a Si/Cr ratio of 40 prepared by the DHT method using a laser line at 458 nm as the exciting source (Vis-Raman). A band at 986 cm^{-1} was detected, but the band was rather broad and the ratio of signal to noise was not so satisfactory. We have recorded Raman spectra of our Cr-MCM-41 samples with excitation at 514 nm, but any useful information could not be obtained because of the serious fluorescence.

It has been clarified that the use of a UV line as exciting source of Raman spectroscopy (UV-Raman) can avoid the fluorescence interference from molecular sieves or related materials [45]. Furthermore, the use of UV excitation may lead to a remarkable increase in the intensity of Raman bands if the resonance occurs, and the UV-resonance Raman spectroscopy has been used to identify the locations of titanium [46,47] and vanadium [48,49] in microporous and mesoporous molecular sieves. In the case of Cr-MCM-41, as shown in Fig. 6, the charge transfer of the $d\pi$–$p\pi$ transition between chromium and oxygen of chromate species occurred from 250 to 500 nm with peaks at 280 and 370 nm. The use of a UV laser of 325 nm as the exciting source in our measurements may cause the resonance. To keep the samples dehydrated, the measurements were performed at 200 °C in pure N_2 gas flow. Fig. 7 shows the UV-Raman spectra of the samples prepared by both the DHT and the TIE methods. No serious interference of the fluorescence was observed in this case. The samples prepared by different methods exhibited remarkable differences in UV-Raman spectra. An intense and sharp band at 980 cm^{-1} was observed for the Cr-MCM-41 samples synthesized by the DHT method, whereas a set of multibands around 1000–1100 cm^{-1} appeared in addition to that at 980 cm^{-1} for the samples by the TIE method. Weckhuysen and co-workers [2] have reviewed the Raman spectra of a number of supported chromium oxides and suggested that the band at 980–990 cm^{-1} could be assigned to the Cr–O stretching of dehydrated monochromate species (CrO_4^{2-}), while those at 1000–1100 cm^{-1} can be ascribed to the Cr–O stretching of dehydrated polychromates. Thus, Fig. 7 strongly suggests that the monochromate mainly exists on the samples synthesized by the DHT method, whereas the samples by the TIE method contain several types of chromate species on the wall surface of MCM-41. For polymolybdates, it is reported that the frequency of the band of Mo=O increases

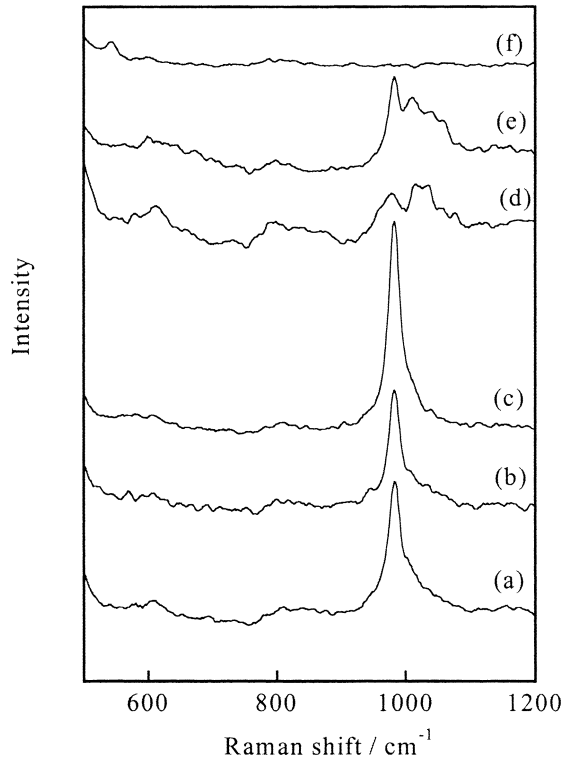

Fig. 7. UV-Raman spectra of the Cr-MCM-41 samples (a–e) and Cr_2O_3 (f). (a) DHT, Si/Cr = 100; (b) DHT, Si/Cr = 50; (c) DHT, Si/Cr = 25; (d) TIE, Si/Cr = 100; (e) TIE, Si/Cr = 50.

as the degree of polymerization increases [50]. Although the structure of polychromates (tetrahedral coordination of Cr) is different from that of polymolybdates (octahedral coordination of Mo), it is reasonable that the frequency of the Cr–O stretching of polychromate also increases with the degree of polymerization. We thus tentatively propose that the multibands observed at 1000–1100 cm^{-1} correspond to the dehydrated polychromates with different degrees of polymerization, e.g., dichromate, trichromate, and tetrachromate. It is worth noting that the chromium in either monochromate or polychromate is tetrahedrally coordinated with oxygen. For Cr_2O_3, in which chromium is in octahedral coordination and the CrO_6 octahedra are linked with each other, no band at 900–1200 cm^{-1} has been observed as shown in Fig. 7 (curve f). Therefore, UV-Raman spectroscopy is a potent tool in distinguishing the chromate species with different degrees of polymerization on the wall surface of MCM-41.

3.3. Catalytic properties of Cr-MCM-41

Fig. 8 shows the catalytic properties of Cr-MCM-41 samples synthesized by both methods in the dehydrogenation of C_3H_8 with CO_2 at 823 K. The two types of catalysts showed very similar catalytic behaviors. The conversion of C_3H_8 increased almost linearly with an increase in chromium content in both cases, strongly suggesting that chromium is the active site for the reaction. Although the BET surface area and pore volume decreased largely as the chromium content increased to 3.4 wt% (Si/Cr = 25, Table 1), the conversion of C_3H_8 and the yield to C_3H_6 still increased with chromium content, indicating that such change in the porous properties did not significantly influence the catalytic behavior in dehydrogenation of C_3H_8. The selectivity to C_3H_6 was kept at 92–95%, and the yield of C_3H_6 was ca. 26% over the sample with a chromium content of 3.4 wt% prepared by either method. The result obtained here is remarkably higher than those reported over the chromium oxides supported on Al_2O_3, active carbon, and SiO_2 [7], where similar reaction conditions were employed.

In order to clarify the contribution of CO_2 to the reaction, the effect of the partial pressure of CO_2 has been investigated over the DHT and the TIE samples with a Si/Cr ratio of 50 (Cr content of 1.7 wt%) and the results are shown in Fig. 9. Similar profiles were obtained for both types of catalysts. Although the dehydrogenation of C_3H_8 also occurred in the absence of CO_2, the conversion of C_3H_8 increased remarkably with an increase of the partial pressure of CO_2. The presence of CO_2 also slightly increased the selectivity to C_3H_6. Two possibilities have been proposed for explaining the enhancing effect of CO_2 on the dehydrogenation of lower alkanes such as C_2H_6 and C_3H_8 over several catalysts. The presence of CO_2 was found to reduce the carbon deposition and to assist in the rapid desorption of C_2H_4 from the catalyst surface in the dehydrogenation of C_2H_6 over a Ga_2O_3/TiO_2 [51]. One of the present authors

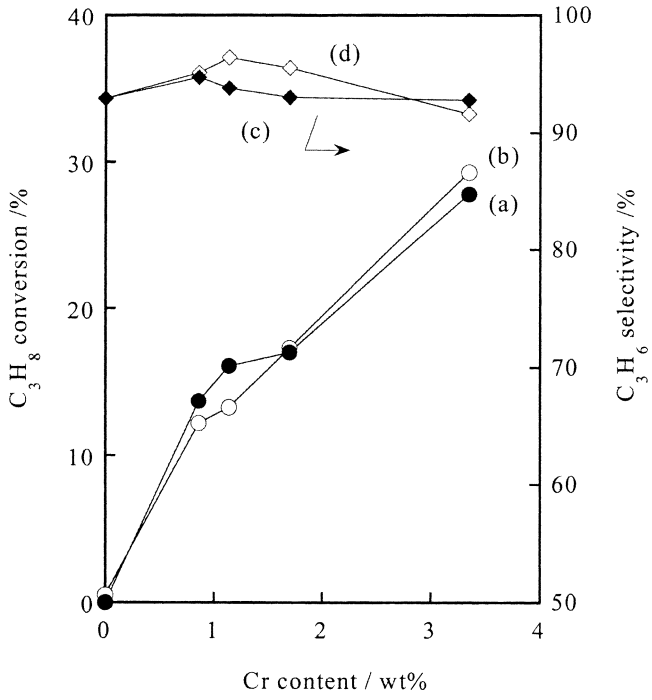

Fig. 8. Dehydrogenation of C_3H_8 with CO_2 over the Cr-MCM-41 samples prepared by DHT (a, c) and TIE (b, d) methods. (a and b) C_3H_8 conversion, (c and d) C_3H_6 selectivity. Reaction conditions: catalyst weight, 0.4 g; $P(C_3H_8) = 12.2$ kPa; $P(CO_2) = 68.9$ kPa; $T = 823$ K; $F = 0.134$ mol(STP) h^{-1}.

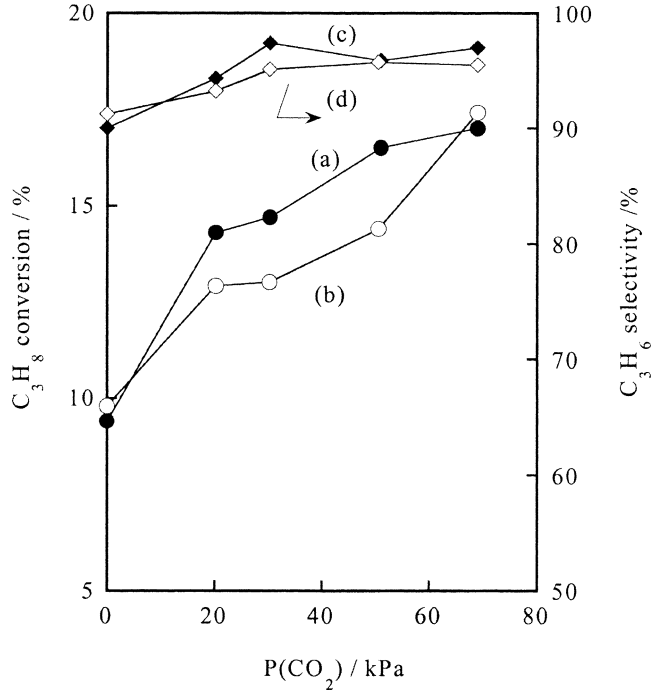

Fig. 9. Effect of partial pressure of CO_2 on the dehydrogenation of C_3H_8 over the Cr-MCM-41 samples with Si/Cr ratio of 50 prepared by DHT (a, c) and TIE (b, d) methods. (a and b) C_3H_8 conversion, (c and d) C_3H_6 selectivity. Reaction conditions: catalyst weight, 0.4 g; $P(C_3H_8) = 12.2$ kPa; $T = 823$ K; $F = 0.134$ mol(STP) h^{-1}.

Table 3
Comparison of the catalytic properties of the Cr-MCM-41 samples by the DHT and the TIE methods in the oxidation of methane with oxygen

Catalyst	Temperature (K)	CH_4 conversion (%)	HCHO selectivity (%)	HCHO formation rate (mmol h^{-1} g^{-1})
DHT Si/Cr = 100	723	0.42	40.2	1.81
	773	2.51	22.5	6.05
DHT Si/Cr = 50	723	0.78	27.2	2.27
	773	5.25	12.7	7.15
DHT Si/Cr = 25	723	0.93	19.2	1.91
	773	6.80	6.5	4.74
TIE Si/Cr = 100	723	0.25	11.0	0.29
	773	2.34	4.0	1.00
TIE Si/Cr = 50	723	0.50	1.4	0.075
	773	4.01	0.5	0.21
TIE Si/Cr = 25	723	0.62	1.0	0.065
	773	4.78	0.5	0.25

Reaction conditions: catalyst weight, 0.05 g; $P(CH_4) = P(O_2) = 16.9$ kPa, He was used as balance gas; F(total) = 0.321 mol(STP) h^{-1}.

identified that CO_2 could act as oxidant for the coupling of CH_4 to C_2 hydrocarbons over a variety of binary oxides [52–54]. It has recently been reported that CO_2 may provide oxygen species for the dehydrogenation of C_2H_6 over a supported Cr_2O_3 [55] and C_3H_8 over a $NiMoO_4$ catalyst [56]. We speculate that these two roles of CO_2, i.e., the reduction of carbon deposition and the donation of oxygen species, may both account for the enhancement of dehydrogenation of C_3H_8 to C_3H_6 over the current catalysts.

Table 3 compares the catalytic properties of the Cr-MCM-41 synthesized by the two methods in the partial oxidation of CH_4 at 723 and 773 K with oxygen. HCHO, the partial oxidation product, was formed along with CO and CO_2 over each sample. The conversion of CH_4 increased remarkably with rising reaction temperatures, but the selectivity to HCHO decreased largely at the same time. The increase in chromium content also increased the conversion of CH_4 and decreased the selectivity to HCHO over both types of catalysts. The comparison of the DHT sample with the TIE one containing the same chromium content shows that the former type of catalyst exhibits remarkably higher selectivity to HCHO and higher conversion of CH_4 under the same reaction conditions. Although the highest rate of HCHO formation over the Cr-MCM-41-DHT (ca. 7 mmol g^{-1} h^{-1} at 773 K, Si/Cr = 50) was lower than that over a MCM-41-supported vanadium oxide (ca. 35 mmol g^{-1} h^{-1} at 868 K) [57], the Cr-MCM-41-DHT catalyst could operate at lower temperatures. Furthermore, to the best of our knowledge, this is the first example that HCHO could be produced with significant amounts on the supported chromium catalyst. The previous study found that the oxidation of CH_4 over the supported chromium oxide such as CrO_x/SiO_2 resulted in complete combustion of CH_4, although the CrO_x/SiO_2 showed the highest conversion of CH_4 among CrO_x/SiO_2, VO_x/SiO_2, and MoO_x/SiO_2 [2].

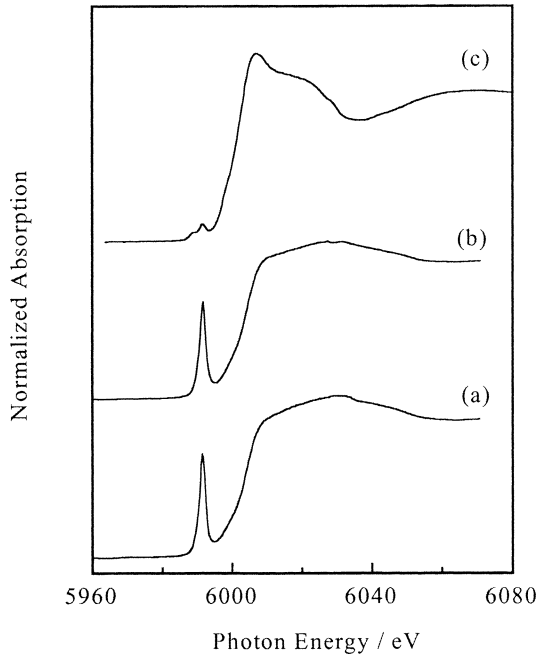

Fig. 10. CrK-edge XANES spectra of the Cr-MCM-41-DHT sample with Si/Cr ratio of 50: (a) after calcination, (b) after pretreatment with He, (c) after dehydrogenation reaction under the conditions in Fig. 8 for 5 h.

3.4. Characterization of Cr-MCM-41 after catalytic reactions

XRD measurements for the Cr-MCM-41 samples after both reactions revealed that the mesoporous structure did not undergo significant change.

In order to gain insight into the change of the coordination structure of chromium, the Cr-MCM-41-DHT sample with a Si/Cr ratio of 50 was characterized after the dehydrogenation of C_3H_8 in the presence of CO_2. Figs. 10 and 11 show the XANES patterns and the Fourier transforms of EXAFS after calcination, the pretreatment in He flow at 823 K, and the reaction under the conditions shown in Fig. 8 for 5 h. After pretreatment with He for 1 h at 823 K, the curves in both

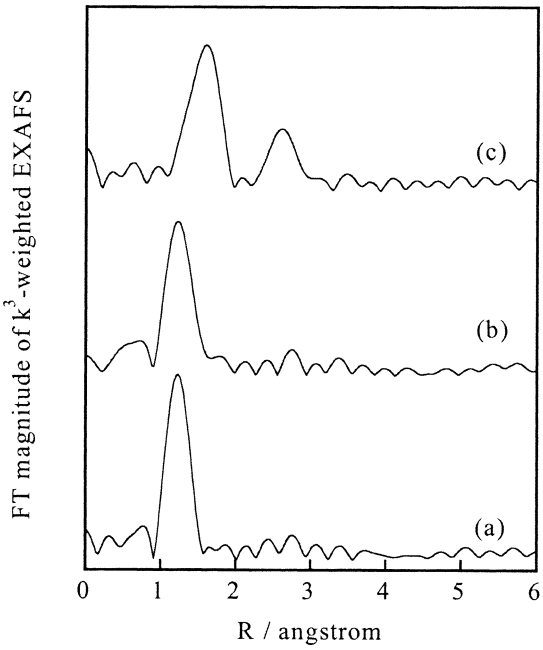

Fig. 11. Fourier transforms of k^3-weighted CrK-edge EXAFS of the Cr-MCM-41-DHT sample with Si/Cr ratio of 50: (a) after calcination, (b) after pretreatment with He, (c) after dehydrogenation reaction under the conditions in Fig. 8 for 5 h.

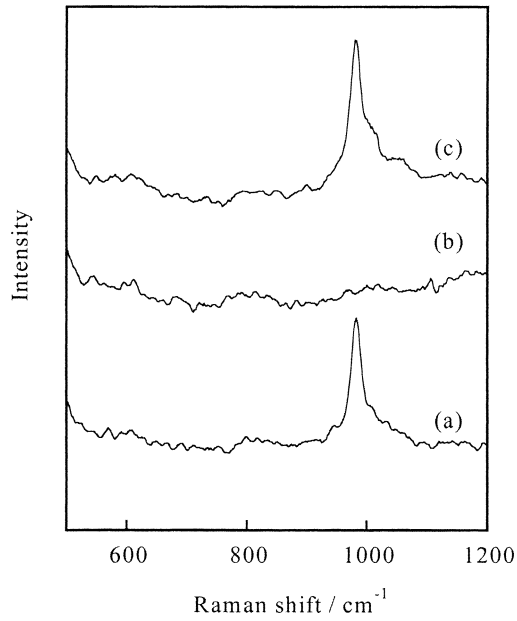

Fig. 12. UV-Raman spectra of the Cr-MCM-41-DHT sample with Si/Cr ratio of 50: (a) after calcination, (b) after dehydrogenation reaction under the conditions in Fig. 8 for 5 h, (c) after partial oxidation of CH_4 under the conditions in Table 3 for 5 h.

figures did not undergo significant change. However, the XANES pattern and the EXAFS curve changed significantly after the dehydrogenation of C_3H_8 in the presence of CO_2. Fig. 10 shows that, after reaction, the XANES preedge peak became very weak, and the edge position shifted to lower energy, suggesting that the chromium has been changed from Cr(VI) in tetrahedral coordination to Cr(III) in octahedral coordination. For the EXAFS result (Fig. 11), two distinct peaks were observed at 1.60 and 2.63 Å (non-phase-shift corrected) after the reaction. Similar peaks were also observed for Cr_2O_3 (curve a in Fig. 4), and as described above these two peaks could be assigned to the bonds of Cr–O in CrO_6 octahedra and Cr–O–Cr through edge-shared CrO_6 octahedra. However, the peak at ca. 3.29 Å (non-phase-shift corrected) for Cr_2O_3 was not observable for the sample after the reaction, and the peak at 2.63 Å (non-phase-shift corrected) was relatively weaker as compared with that for Cr_2O_3. Thus, it is reasonable to consider that the chromium species exist as small $Cr^{III}O_x$ clusters after the dehydrogenation reaction, although it is difficult to determine the size of these clusters [58]. The curve-fitting results for Cr–O shell shown in Table 2 confirmed that the coordination structure of chromium was changed from tetrahedral to octahedral after 5 h of reaction of C_3H_8 dehydrogenation in the presence of CO_2. Further studies revealed that the transformation of tetrahedral Cr(VI) to octahedral Cr(III) occurred even after the reaction for 0.5 h. Moreover, the Cr(VI) species could not be recovered by flowing pure CO_2 at 823 K. In other words, the reoxidation of the reduced Cr(III) could not proceed with CO_2. Similar results were also obtained for the Cr-MCM-41-TIE sample with a Si/Cr ratio of 50.

UV-Raman spectra for the DHT sample with a Si/Cr ratio of 50 after the dehydrogenation of C_3H_8 and the partial oxidation of CH_4 are shown in Fig. 12. After the dehydrogenation of C_3H_8 in the presence of CO_2, the band at 980 cm^{-1} disappeared. Because no band was observed for Cr_2O_3 at 900–1200 cm^{-1}, the disappearance of the band at 980 cm^{-1} coincided with the XANES and EXAFS results, suggesting the transformation of coordination of chromium from tetrahedron to octahedron. On the other hand, the band at 980 cm^{-1} was not significantly changed after the partial oxidation of CH_4 with O_2. This indicates that the tetrahedral coordination structure of chromium is kept during the partial oxidation of CH_4 with O_2.

3.5. Relationship between catalytic property and coordination structure of chromium

The fast reduction of Cr(VI) to Cr(III) over alumina-supported chromia under a C_3H_8 stream has been detected by Weckhuysen and co-workers [29] using in situ UV–vis diffuse reflectance spectroscopy through an optical fiber placed in the catalyst bed. The same authors also confirmed that the turnover frequency for the dehydrogenation of C_3H_8 was higher for multinuclear Cr(III) than for isolated Cr(III) sites [59]. In our case, as described above, we found that the chromate species, either monochromate or polychromate species on the wall surface of MCM-41, were reduced to aggregated $Cr^{III}O_x$ species after the dehydrogenation of C_3H_8 in the presence of CO_2. It is thus reasonable to speculate that such aggregated Cr(III) species are responsible for the dehydrogenation of C_3H_8. Although the difference in the coordination structure of chromium between the TIE and the

DHT samples was remarkable before reaction as shown by the UV-Raman spectroscopy, these chromate species were all transformed to aggregated Cr(III) oxides during the dehydrogenation. We think that this can explain the reason that the DHT and the TIE samples exhibit almost the same catalytic behavior in the dehydrogenation of C_3H_8.

On the other hand, the chromate species of tetrahedral coordination were not significantly changed after the partial oxidation of CH_4 with O_2. The oxidative atmosphere is believed to have kept the high oxidation state of chromium and the coordination structure. Haller and co-workers [31] have reported that the reduced Cr(III) with octahedral coordination in MCM-41 or MCM-48 could easily be reoxidized to tetrahedral Cr(VI) with air. The chromate species with tetrahedral Cr(VI) on MCM-41 may thus be responsible for the activation and the conversion of CH_4. As described above, UV-Raman spectroscopy has elucidated that the degrees of the polymerization of the chromates over the DHT and the TIE samples are different. Monochromate species is mainly detected over the DHT samples, whereas polychromates such as di-, tri-, and tetra-chromates also exist over the TIE samples besides the monochromate. This must result in different catalytic behaviors of the two types of samples in the oxidation of CH_4 with O_2. The remarkably higher selectivity to HCHO over the DHT samples indicates that the monochromate species, which are highly isolated on the wall surface of MCM-41, account for the formation of partial oxidation product, i.e., HCHO. The samples by the TIE method, which contained polychromates, only gave much lower selectivity to HCHO and produced mainly carbon oxides.

4. Conclusions

Chromium could be introduced into MCM-41 by direct hydrothermal synthesis and template-ion exchange without destroying the mesoporous structure of MCM-41 if the Si/Cr ratio was kept higher than 25. The DHT method results in monochromate species on the wall surface of MCM-41, whereas polychromate species exist in large quantity besides the monochromate over the samples by the TIE method. The two types of samples exhibit similar catalytic property in the dehydrogenation of propane with carbon dioxide. High selectivity and yield to propylene have been achieved and the presence of carbon dioxide remarkably enhances the reaction. On the other hand, a distinct difference in catalytic behavior for the partial oxidation of methane with oxygen has been observed between the two series of samples. The samples by the DHT method provide formaldehyde with higher selectivity at higher methane conversion than those by the TIE method. It has been elucidated that the chromate species over both types of samples are reduced to aggregated Cr(III) oxide clusters during the dehydrogenation of propane, while they are kept during the oxidation of methane. This is proposed to account for the different behaviors of the two kinds of samples in the two catalytic reactions.

Acknowledgments

This work was supported by the National Natural Science Foundation of China (Nos. 20273054 and 20021002), the Chinese Ministry of Science and Technology (No. G1999022408), and the Scientific Research Foundation for the Returned Overseas Chinese Scholars, State Education Ministry, and the Creative Research Foundation for Young Scientists by Fujian Province of China. The X-ray absorption measurements were performed under the approval of the Photon Factory (KEK-PF) Program Advisory Committee (Proposal No. 2002G097).

References

[1] J. Muzart, Chem. Rev. 92 (1992) 113.
[2] B.M. Weckhuysen, I.E. Wachs, R.A. Schoonheydt, Chem. Rev. 96 (1996) 3327.
[3] M. MacDaniel, Adv. Catal. 33 (1985) 47.
[4] T.J. Pullukat, R.E. Hoff, Catal. Rev. Sci. Eng. 41 (1999) 389.
[5] L.R. Mentasty, O.F. Gorriz, L.E. Cadus, Ind. Eng. Chem. Res. 38 (1999) 396.
[6] A. Hakuli, M.E. Harlin, L.B. Backman, A.O.I. Krause, J. Catal. 184 (1999) 349.
[7] I. Takahara, W.C. Chang, N. Mimura, M. Saito, Catal. Today 45 (1998) 55.
[8] S. Wang, K. Murata, S. Hayakawa, K. Suzuki, Appl. Catal. A 196 (2000) 1.
[9] X. Ge, M.M. Zhu, J.Y. Shen, React. Kinet. Catal. Lett. 77 (2002) 103.
[10] B. Crzybowska, J. Sloczynski, R. Grabowski, K. Wcislo, A. Kozlowska, J. Stoch, J. Zielinski, J. Catal. 178 (1998) 687.
[11] A. Jimenez-Lopez, E. Rodriguez-Castellon, P. Maireles-Torres, L. Diaz, J. Merida-Robles, Appl. Catal. A 218 (2001) 295.
[12] S.M. Al-Zahrani, N.O. Elbashir, A.E. Abasaeed, M. Abdulwahed, Ind. Eng. Chem. Res. 40 (2001) 781.
[13] M. Cherian, M.S. Rao, A.M. Hirt, I.E. Waches, G. Deo, J. Catal. 211 (2002) 482.
[14] C.M. Pradier, F. Rodrigues, P. Marcus, M.V. Landau, M.L. Laliya, A. Gutman, M. Herskowitz, Appl. Catal. B 27 (2000) 73.
[15] M.L. Parentis, N.A. Bonini, E.E. Gonzo, React. Kinet. Catal. Lett. 76 (2002) 243.
[16] D. Trong On, D. Desplantier-Giscard, C. Danumah, D. Kaliaguine, Appl. Catal. A 222 (2001) 299.
[17] N. Ulagappan, C.N.R. Rao, Chem. Commun. (1996) 1047.
[18] W. Zhang, T.J. Pinnavaia, Catal. Lett. 38 (1996) 261.
[19] Z. Zhu, Z. Chang, L. Kevan, J. Phys. Chem. B 103 (1999) 2680.
[20] J.S. Gonzalez, J.M. Robles, M.A. Rodriguez, P.M. Torres, E.R. Castellon, A.J. Lopez, Catal. Lett. 64 (2000) 209.
[21] D. Wei, N. Yao, G.L. Haller, Stud. Surf. Sci. Catal. 121 (1999) 239.
[22] A. Sakthivel, P. Selvam, J. Catal. 211 (2002) 134.
[23] W.A. Carvalho, P.B. Varaldo, M. Wallau, U. Schuchardt, Zeolites 18 (1997) 408.
[24] R.A. Sheldon, M. Wallau, I.W.C.E. Arends, U. Schuchardt, Acc. Chem. Res. 31 (1998) 485.
[25] I.W.C.E. Arends, R.A. Sheldon, Appl. Catal. A 212 (2001) 175.

[26] H. Yamashita, K. Yoshizawa, M. Ariyuli, S. Higashimoto, M. Anpo, Stud. Surf. Sci. Catal. 141 (2002) 495.
[27] X.Z. Zhang, Y.H. Yue, Z. Gao, Catal. Lett. 83 (2002) 19.
[28] S. Khaddar-Zine, A. Ghorbel, C. Naccache, J. Mol. Catal. A 150 (1999) 223.
[29] R.L. Puurunen, B.G. Beheydt, B.M. Weckhuysen, J. Catal. 204 (2001) 253.
[30] J.R. Sohn, S.G. Ryu, Catal. Lett. 74 (2001) 105.
[31] C. Pak, G.L. Haller, Micropor. Mesopor. Mater. 48 (2001) 165.
[32] J.M. Kanervo, A.O.I. Krause, J. Phys. Chem. B 105 (2001) 9778.
[33] B.M. Weckhuysen, Chem. Commun. (2002) 97.
[34] Q. Zhang, Y. Wang, Y. Ohishi, T. Shishido, K. Takehira, J. Catal. 202 (2001) 308.
[35] Y. Wang, Q. Zhang, T. Shishido, K. Takehira, J. Catal. 209 (2002) 186.
[36] Q. Zhang, Y. Wang, S. Itsuki, T. Shishido, K. Takehira, J. Mol. Catal. A 188 (2002) 189.
[37] N. Lang, P. Delichere, A. Tuel, Micropor. Mesopor. Mater. 56 (2002) 203.
[38] A.B. Bourlinos, M.A. Karakassides, D. Petridis, J. Phys. Chem. B 104 (2000) 4375.
[39] M. Yonemitsu, Y. Tanaka, M. Iwamoto, Chem. Mater. 9 (1997) 2679.
[40] M. Iwamoto, Y. Tanaka, Catal. Surv. Jpn. 5 (2001) 25.
[41] A. Badiei, L. Bonneviot, Inorg. Chem. 37 (1998) 4142.
[42] D. Dollimore, G.R. Heal, J. Appl. Chem. 14 (1964) 109.
[43] J.-H. Choy, J.-B. Yoon, D.-K. Kim, S.-H. Hwang, Inorg. Chem. 34 (1995) 6524.
[44] Y. Ma, S.L. Suib, T. Ressler, J. Wong, M. Lovallo, M. Tsapatsis, Chem. Mater. 11 (1999) 3545.
[45] C. Li, P.C. Stairs, Stud. Surf. Sci. Catal. 101 (1996) 881.
[46] C. Li, G. Xiong, J. Liu, P. Ying, Q. Xin, Z. Fen, J. Phys. Chem. B 105 (2001) 2993.
[47] G. Ricchiardi, A. Damin, S. Bordiga, C. Lamberti, G. Spanò, F. Rivetti, A. Zecchina, J. Am. Chem. Soc. 123 (2001) 11409.
[48] G. Xiong, L. Can, H. Li, Q. Xin, Z. Feng, Chem. Commun. (2000) 677.
[49] D. Wei, H. Wang, X. Feng, W. Chueh, P. Ravikovitch, M. Lyubovsky, C. Li, T. Takeguchi, G.L. Haller, J. Phys. Chem. B 103 (1999) 2113.
[50] G. Mestl, T.K.K. Srinivasan, Catal. Rev. Sci. Eng. 40 (1998) 451.
[51] K. Nakagawa, C. Kajita, K. Okumura, N. Ikenaga, M. Nishitani-Gamo, T. Ando, T.T. Kobayashi, T. Suzuki, J. Catal. 203 (2001) 87.
[52] Y. Wang, Y. Takahashi, Y. Ohtsuka, J. Catal. 186 (1999) 160.
[53] Y. Wang, Y. Ohtsuka, J. Catal. 192 (2000) 252.
[54] Y. Wang, Y. Ohtsuka, Appl. Catal. A 219 (2001) 183.
[55] K. Nakagawa, C. Kajita, N. Ikenaga, T. Suzuki, T. Kobayashi, M. Nishitani-Gamo, T. Ando, J. Phys. Chem. B 107 (2003) 4048.
[56] F. Dury, E.M. Gaigneaux, P. Ruiz, Appl. Catal. A 242 (2003) 187.
[57] H. Berndt, A. Martin, A. Brückner, E. Schreier, D. Müller, H. Kosslick, G.-U. Wolf, B. Lücke, J. Catal. 191 (2000) 384.
[58] D.J. Jones, J. Rozière, P. Maireles-Torres, A. Jiménez-López, P. Plivera-Pastor, E. Rodríguez-Castellón, A.A.G. Tomlinson, Inorg. Chem. 34 (1995) 4611.
[59] R.L. Puurunen, B.M. Weckhuysen, J. Catal. 210 (2002) 418.